Inferring the interplanetary dust properties

Jérémie Lasue, Anny Chantal Levasseur-Regourd, Nicolas Fray, Hervé Cottin

A&A 473, 641–649 (2007)
DOI: 10.1051/0004-6361:20077623

Astronomy & Astrophysics

Inferring the interplanetary dust properties

from remote observations and simulations

J. Lasue[1], A. C. Levasseur-Regourd[1,2], N. Fray[3], and H. Cottin[3]

[1] Service d'aéronomie-IPSL-CNRS, UMR 7620, Route des Gâtines, BP 3, 91371 Verrières-le-Buisson, France
e-mail: jeremie.lasue@aerov.jussieu.fr
[2] Université Pierre et Marie Curie-Paris6, Service d'aéronomie UMR 7620, 75005 Paris, France
e-mail: chantal.levasseur-regourd@aerov.jussieu.fr
[3] Laboratoire Interuniversitaire des Systèmes Atmosphériques, UMR 7583, Universités Paris 7 et Paris 12, 61 Av. du Général de Gaulle, 94010 Créteil, France
e-mail: [fray;cottin]@lisa.univ-paris12.fr

Received 10 April 2007 / Accepted 25 June 2007

ABSTRACT

Context. Since in situ studies and interplanetary dust collections only provide a spatially limited amount of information about the interplanetary dust properties, it is of major importance to complete these studies with properties inferred from remote observations of scattered and emitted light, with interpretation through simulations.
Aims. Physical properties of the interplanetary dust in the near-ecliptic symmetry surface, such as the local polarization, temperature, and composition, together with their heliocentric variations, may be derived from scattered and emitted light observations, giving clues to the respective contribution of the particle sources.
Methods. A model of light scattering by a cloud of solid particles constituted by spheroidal grains and aggregates thereof is used to interpret the local light-scattering data. Equilibrium temperature of the same particles allows us to interpret the temperature heliocentric variations.
Results. A good fit of the local polarization phase curve, P_α, near 1.5 AU from the Sun is obtained for a mixture of silicates and more absorbing organic material (≈40% in mass) and for a realistic size distribution typical of the interplanetary dust in the 0.2 μm to 200 μm size range. The contribution of dust particles of cometary origin is at least 20% in mass. The same size distribution of particles gives a dependence of the temperature with the solar distance, R, in $R^{-0.45}$ that is different than the typical black body behavior. The heliocentric dependence of $P_{\alpha=90^\circ}$ is interpreted as a progressive disappearance of solid organic (such as HCN polymers or amorphous carbon) towards the Sun.
Conclusions.

Key words. interplanetary medium – polarization – radiation mechanisms: thermal – methods: numerical

1. Introduction

Describing the particles constituting the interplanetary dust cloud (IDC) in terms of morphology, porosity, size distribution, and complex refractive indices offers a clue to their origin and evolution. Information can be retrieved through (a few) in situ studies (see e.g. Jessberger et al. 2001) and through remote observations of the light-scattering properties (brightness and polarization of solar light scattered by the dust particles in the visible domain) and emissivity (in the infrared spectrum) of the dust cloud; see e.g. Levasseur-Regourd et al. (1999). Photometric measurements integrate all the local contributions emitted and scattered by the dust along the line of sight. Consequently, techniques of inversion, such as the "nodes of lesser uncertainty" method (see e.g. Dumont & Levasseur-Regourd 1988; Levasseur-Regourd et al. 2001, and references therein) are needed to retrieve the local properties. All the values given in the following text correspond to bulk values deduced from inversion methods over elementary volumes.

Light-scattering numerical simulations can be used to derive physical properties of clouds of dust particles, typically of comet origin (see e.g. Levasseur-Regourd et al. 2007, and references therein). Realistic light-scattering models for a distribution of particles constituted of a mixture of spheroidal grains and aggregates of small spheroids have already been used to derive information about the composition and size distribution (lower and upper cut-off, power law coefficient, proportion of absorbing and non-absorbing material, and proportion of aggregates) in the case of comet Hale-Bopp dust polarimetric observations (Lasue & Levasseur-Regourd 2006).

This study presents the results obtained by applying an irregular particle cloud model in the case of the interplanetary dust cloud observations to estimate the physical properties of the size distribution and the proportion of fluffy particles. It tentatively indicates the relative contribution of particles from cometary and asteroidal origins. In the next two sections, clues to the properties of the interplanetary dust cloud and source particles are reviewed. In the last two sections, the emitted light and local temperature properties of the cloud are analyzed through our model.

2. Local properties of the interplanetary dust cloud

2.1. Scattered light

The local albedo of the interplanetary dust cloud, A, approximately follows $A = (0.07 \pm 0.03)\, R^{-0.34\pm0.05}$ in the near-ecliptic

symmetry surface as a function of the solar distance, R, between 1.5 and 0.5 AU, as deduced from the brightness observations in the visible (Dumont & Levasseur-Regourd 1988; Levasseur-Regourd et al. 2001).

The local polarization, P, cannot be estimated at all the phase angles and solar distances. With the "nodes of lesser uncertainty" method, two zones can be described. The radial node gives information on the polarization at 90° of phase angle with a varying solar distance, whereas the Martian node located at 1.5 AU from the Sun gives the variation in P with the phase angle (Dumont & Levasseur-Regourd 1988). The deduced phase curve presents a similar shape to the ones observed for comets and other dusty objects in the Solar System, with large error bars due to inversion methods at a single wavelength $\lambda = 550$ nm and with a shape typical of the interaction of light with irregular particles comparable in size to the wavelength (see e.g. Mann 1992; Lumme 2000; Levasseur-Regourd & Hadamcik 2003). The phase curve is smooth with a small negative branch below the inversion angle, $\alpha_0 \approx 15° \pm 2°$ and a large positive branch, with a value $P_{90°} \approx 30\% \pm 3\%$.

From the observational data, no significant variation in P with the wavelength, λ, can be noticed, as shown by Leinert et al. (1998); however, a heliocentric dependence of $P_{90°}$ between 1.5 and 0.5 AU can be pointed out (Lumme 2000; Levasseur-Regourd et al. 2001):

$$P_{90°} = (0.30 \pm 0.03)\, R^{0.5\pm0.1}. \quad (1)$$

This relation suggests that a change either in the physical properties or in the chemical composition of the particles is required to interpret the observed solar distance dependence of the IDC local polarization.

2.2. Temperature

Although the absolute temperature values may not be accurately determined, the variation in local temperature of the IDC with the solar distance is well-constrained. The dependence of T on R closely follows a power law, the exponent, t, (hereafter called temperature-distance factor), which is not as steep as the one expected from a black body (T proportional to $\frac{1}{\sqrt{R}}$):

$$T = (250 \pm 10\ \mathrm{K})\, R^{-0.36\pm0.03}. \quad (2)$$

This relation is approximately valid between 1.5 and 0.5 AU as deduced from the infrared observations (Dumont & Levasseur-Regourd 1988; Reach 1991; Renard et al. 1995; Levasseur-Regourd et al. 2001).

3. Clues to the properties of source particles

The IDC, as probed around 1 AU, originates from at least three different sources: fluffy and easily fragmenting particles of cometary origin (see e.g. Whipple 1951), asteroidal dust made of compact particles produced by asteroidal shattering (see e.g. Jessberger et al. 2001), and to a lesser extent elongated submicron interstellar grains passing through the solar system and a priori not directly linked to the primordial grains that formed the solar system and grains coming from the Jovian system (see e.g. Grün et al. 1993).

3.1. Sizes of the particles

The size distribution of compact or fluffy particles resulting from particle-particle collisions is expected to follow a power law, a^s, where the effective diameter, a, is the diameter of the sphere with a volume equivalent to the one of the irregular particle, and where s is equal to −3 from theoretical calculations (Hellyer 1970) and is between −3.5 and −3 from experimental simulations (see e.g. Mukai et al. 2001). Observations of the solid component of the cometary comæ have shown that such a coefficient is close to −3 (e.g. -3.1 ± 0.3 from Rosetta observations of comet 9P/Tempel 1 after the Deep Impact event by Jorda et al. 2007). In situ measurements within the IDC suggest s is around −3 for particles smaller than 20 μm and equal to −4.4 for larger particles (Grün et al. 2001).

So-called IDPs, i.e. interplanetary dust particles collected in the Earth's stratosphere, typical size ranges from 5 μm to 25 μm (Jessberger et al. 2001). For the IDPs presenting an aggregated structure and possibly originating from comets, the constituent grains have a mean size around 0.3 μm. Evidence of such a fluffy structure has also been shown from the study of the aluminium craters and aerogel penetration tracks from the Stardust samples (Hörz et al. 2006). The larger micrometeorites, collected in the polar regions or at the bottom of the oceans, have sizes ranging from 20 μm to 1 mm, and because of their large size, they are usually compact due to melting during their entry through the Earth's atmosphere (Engrand & Maurette 1998).

3.2. Optical constants of the particles

Studies of comets, IDPs, and micrometeorites have shown the predominance of silicates and "CHON" materials in the composition of extraterrestrial particles (Hanner & Bradley 2004). Precise spectroscopic studies of silicates have shown the presence of both amorphous and crystalline silicates consisting of olivine or pyroxene that could be explained by radial mixing of the elements in the early solar nebula (Bockelée-Morvan et al. 2002). Models of comets (Wooden et al. 1999; Hayward et al. 2000), as well as studies of fluffy IDPs (see e.g. Bradley et al. 1992), have shown that the main constituent of the silicates was actually Mg-rich pyroxene with a contribution between 60% and 90% and an absorption between 0.001 and 0.01 in the visible domain near 550 nm (as expressed in terms of the imaginary part, k, of the optical index $m = n+ik$, Dorschner et al. 1995). The recent mineralogical studies of the Stardust samples have also confirmed a variety of olivine and pyroxene silicates in various crystallization states as the main component (Zolensky et al. 2006). In the visible domain, the crystalline silicates present approximately the same optical indices as the amorphous, glassy silicates with an absorption $k \approx 0.0001$ (Jäger et al. 1998; Lucey 1998). It may thus be assumed that amorphous and crystalline silicates have similar optical indices in the visible. In this study, the complex index of silicates is assumed to be the one of Mg-rich pyroxene (typically $Mg_xFe_{1-x}SiO_3$ with $0.8 < x < 0.7$ as measured in laboratory by Dorschner et al. 1995), as it represents most of the observed silicates (see Sect. 4.1 for more details).

The "CHON", or the organic component of the particles, is a more absorbing material composed of lighter elements that could appear in cometary dust particles from the heavy radiation processing of ices and light elements deposited on the grains. Attempts to characterize the nature of the carbonaceous fraction in IDPs suggest that amorphous carbon is dominant (Keller et al. 1994). However, recent studies suggest that one half of the carbon contained in typical IDPs is present in the form of organic carbon (Flynn et al. 2004). Laboratory experiments of radiation processing of ices have been shown to produce absorbing organic material with a high real part of the optical index (close to 2) and imaginary part between 0.1 to 0.4, see e.g.

Jenniskens (1993) and Li & Greenberg (1997). Studies of deposited graphite gave optical index values in the visible on the order of 1.71 + i 0.1 (Papoular et al. 1993). The amorphous carbon presents a very high absorption with an optical index in the visible of 1.88 + i 0.71 (Edoh 1983). In this study, the complex index of organic material taken from Li & Greenberg (1997) is assumed to reproduce the behavior of irradiated cometary ices, and the complex index of amorphous carbon is taken from Edoh (1983).

The spectrum of the zodiacal light is similar to the solar spectrum (see e.g. Levasseur-Regourd et al. 2001), and it peaks around 550 nm. As a first approximation, for the calculations of light scattering, the complex index of the particles is taken around this particular wavelength. However, since equilibrium temperature calculations take the infrared emission of the particles into account, the variation in the complex index with the wavelength will be taken into account for these calculations.

3.3. Shapes of the particles

The IDC particles ejected by comets are probably very irregular with both compact and aggregated ones, as shown from light scattering studies (Lasue & Levasseur-Regourd 2006) and the study of foil craters and the aerogel penetration tracks of Stardust (Hörz et al. 2006). Following the "bird-nest" model proposed by Greenberg & Hage (1990), the aggregates are assumed to be built of spheroidal grains with an axis ratio around 2. Such grains might be expected to have a layered structure, such as a silicates-core covered by an organic-mantle, with a material ratio similar to what is expected from protosolar clouds models. These grains of interstellar origin may be used to model the IDC interstellar component.

The IDC particles resulting from asteroidal collisions are probably compact. They may be represented in a first approximation by prolate spheroids with an axis ratio less than 2 as estimated from IDPs collection analysis (Jessberger et al. 2001) and from the experimental simulations of collisions (Mukai et al. 2001). More specifically, the study of Na desorption on meteoroids by Kasuga et al. (2006) has shown that the meteoroids near 1 AU can be large, compact particles.

Finally, following the "bird-nest" model, the interstellar grains present in the interplanetary medium are assumed to be similar to the constituent grains of the aggregated particles described above.

4. Simulation of the scattered light

The variations in the local properties of the dust cloud with the solar distance point to spatial and temporal evolution of the particles, the small particles being ejected by radiation pressure and the largest ones spiralling slowly towards the Sun under the Poynting-Robertson effect (see e.g. Dermott et al. 2001). We now interpret the light scattered and emission results in terms of the properties of the particles through an IDC model using a mixture of fluffy and compact particles composed of silicates and (more absorbing) organic material and possibly amorphous carbon with a model of the IDC including fluffy as well as compact particles constituted from silicates and more absorbing organic material.

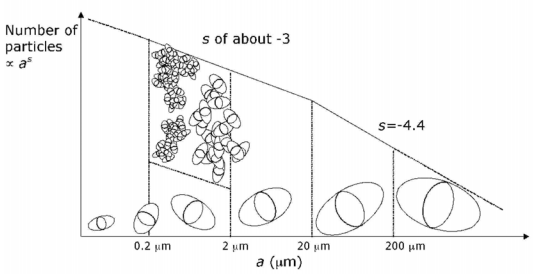

Fig. 1. Size distribution of prolate spheroids (from effective diameter $a = 0.2$ μm to 200 μm) and aggregates thereof (up to 256 spheroids from $a = 0.2$ μm to 2 μm).

4.1. Principle of the calculations

The light-scattering computations are performed for a size distribution of spheroids and aggregates there of following a size distribution similar to the one proposed by Grün et al. (2001) for the in situ measurements of the IDC particles, with two different slopes. The power-law coefficient, s, is around -3 for effective diameters, a, smaller than 20 μm and steeper ($s = -4.4$) for larger effective diameters.

Light scattering by prolate spheroids (axis ratio of 2) is calculated by a code adapted from T-matrix for small spheroids ($a < 3.5$ μm, Mishchenko & Travis 1998) and by ray tracing for large spheroids ($a > 3.5$ μm, Macke & Mishchenko 1996). Contribution of ballistic cluster-cluster aggregates and ballistic particle-cluster aggregates (BCCA and BPCA as defined in Meakin 1983) of up to 256 spheroidal grains calculated with the discrete dipole approximation (DDA) (Draine & Flatau 2000) is taken into account in the cloud for effective diameters of the aggregates, a, between 0.2 μm and 2 μm due to computation limitations. Figure 1 summarizes and illustrates such a size distribution with the mixture of particles.

The brightness, Z, and its two polarized components are calculated by integrating the incident light intensity $Z_{\rm inc}$ over the size distribution, $\Gamma(a)$, of the dust particles and their scattering cross section $\sigma_{\rm sca}(a, \alpha, \lambda)$ at a given phase angle α:

$$Z(\alpha, \lambda) = \frac{\int_0^\infty Z_{\rm inc}(\lambda)\sigma_{\rm sca}(a, \alpha, \lambda)\,\Gamma(a)\,{\rm d}a}{\int_0^\infty \sigma_{\rm sca}(a, \alpha, \lambda)\,\Gamma(a)\,{\rm d}a}\,. \quad (3)$$

Details of the calculations, together with results on comet Hale-Bopp coma composition, are given in Lasue & Levasseur-Regourd (2006). In that paper, the optical properties of particles with a silicates core surrounded by an organic mantle (with expected protosolar abundances) are shown to follow the ones of pure organic particles closely. Fitting the observational data in terms of silicates and organic particles mixture allows us to estimate the range of the carbonaceous material percentage in mass of the IDC, taking into account that organic particles can actually embed silicate material.

Since the light scattered by the particles reproduce the solar spectrum in the visible, for the following calculations we have taken only the complex index of the material near 550 nm as a first approximation of the complex index of the particles. The optical indices are taken to be those of Mg-rich pyroxene (1.62 + i 0.003 at $\lambda = 550$ nm, for $Mg_xFe_{1-x}SiO_3$ with $0.8 < x < 0.7$, Dorschner et al. 1995) and refractive organic material obtained through radiation processing of light elements ($\approx$1.88 + i 0.1 at $\lambda = 550$ nm, Li & Greenberg 1997).

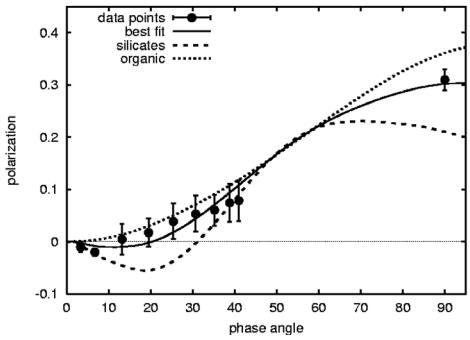

Fig. 2. Zodiacal dust polarization data (•) around 1.5 AU near the symmetry surface and phase curves calculated at 550 nm. Curves are plotted for a realistic interplanetary dust-size distribution of silicates (dashed line), organic (dotted line), and a mixture with ≈40% of organic in mass (thin solid line). Data points are adapted from Levasseur-Regourd et al. (2001) and references therein. The error bars are shown whenever greater than 0.5%.

4.2. Results for the scattered light

Figure 2 presents the phase curves calculated for the IDC size distribution described above. The phase curves obtained for silicates and (absorbing) organic particles are significantly different from each other and from the data points derived from the observations. The organic particles phase curve has a high value P_{90° around 38% and does not show any negative branch, in agreement with previous calculations for absorbing aggregates (Kimura 2001), whereas the silicate-particles phase curve presents a low value P_{90° around 20% and a value α_0 around 30°. Contribution of both absorbing and less-absorbing materials is thus expected to satisfactorily reproduce the IDC composition around 1.5 AU.

As shown in Fig. 2, a good fit of the data retrieved for the polarization phase curve of the IDC near 1.5 AU is obtained for the above-mentioned realistic size distribution with a small-particle power-law coefficient $s = -3.0$ ($s = -4.4$ for large particles as previously defined), effective diameter of 0.22 μm for the lower cutoff and 200 μm for the upper cutoff, and a silicate-organic mixture with about 50% of organic particles in mass. Taking the observational error bars into account, the mass of these organic particles actually comprises between 40% and 60%. When considering that the organic particles in the IDC might embed silicates cores, typically with the cosmic abundances considered in the Greenberg & Hage (1990) model, meaning that these particles actually contain less organic material than is visible, the total amount of organic material can be estimated to be comprised of between 20% and 60% in mass. The amount of aggregates (probably unfragmented particles of cometary origin) is about 20% in mass.

In Fig. 3 are plotted the root mean square values χ^2 of our model compared to the polarization data points, calculated following the equation

$$\chi^2_{\rm pol} = \sum_i \left| \frac{P_{\rm obs}(\alpha_i) - P_{\rm model}(\alpha_i)}{\sigma_P(\alpha_i)} \right|^2 . \quad (4)$$

The plots are shown as 2-dimensional maps as a function of the maximum organic percentage in mass of the cloud and the two other main parameters of the model (small grain size distribution coefficient and cutoff diameter). The first map shows that the size distribution coefficient for small grains (in the 0.2 to 20 μm diameter range) plays an important role for the shape of the phase curve, with a minimum located around -2.95 ± 0.15, thus confirming that a realistic size distribution of the particles should have a coefficient close to this value. The organic percentage in mass is around 50%. The second plot presents the dependence with the minimum diameter and the organic percentage in mass. This shows that the minimum is obtained for a lower cutoff around 0.22 μm. The high variation of the function towards higher values of the lower cutoff shows the predominance of the small particles in the final shape of the polarization phase curve. However too large a lower cutoff can be ruled out because IDPs studies have shown the importance of constituent grains in the 0.1 to 0.3 μm size range as building blocks for interplanetary dust particles. Upper cutoffs larger than 200 μm do not constrain the $\chi^2_{\rm pol}$, so that the larger particles of the size distribution do not influence the shape of the polarization phase curve significantly.

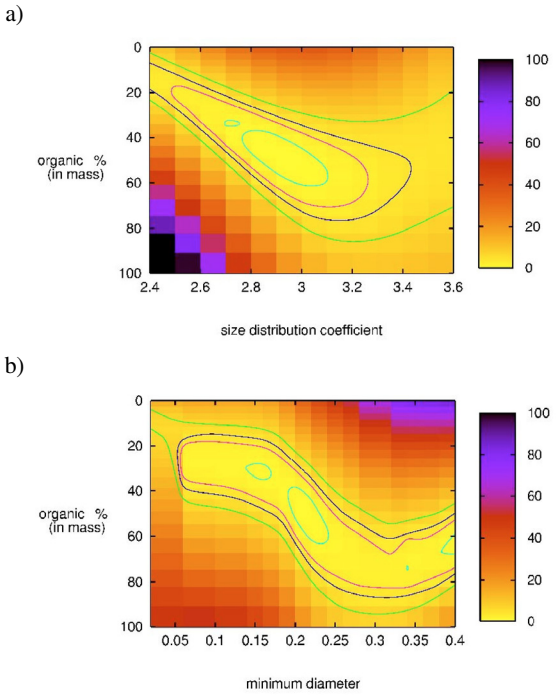

Fig. 3. χ^2 maps of the model compared to the polarization data. a) χ^2 as a function of the maximum organic mass ratio and the small grain size distribution coefficient for a lower diameter of 0.22 μm and b) χ^2 as a function of the maximum organic mass ratio and the small grains' lower diameter for a size distribution power law in $\Gamma(a) = a^{-3}$. The confidence levels curves for 70%, 90%, 95%, and 99% are represented.

In Fig. 4, the dependence of P_{90° on R deduced from the observations (Eq. (1)) is compared to the above model of particles with an organic material percentage varying with the distance to the Sun from 50–100% to 0% as indicated on the curve. The percentage corresponds to the quantity of organic material required to reproduce the variation in the observation's best fit (variation given by Eq. (1), which is more accurate near 1 AU than near 1.5 AU). For a given distance to the Sun the percent range corresponds to the possible existence of core-mantle particles (Lasue & Levasseur-Regourd 2006). A significant loss of organic is mandatory to explain the decrease in P_{90° in the 1.5 to 0.5 AU range. The decrease in P_{90° with R from 1.5 to 0.5 AU could thus be related to a change in the material ratio of the IDC. However, other parameters, such as the size distribution parameters (cutoff diameters or exponent s), could also change with the distance to the Sun when considering small distances to the Sun

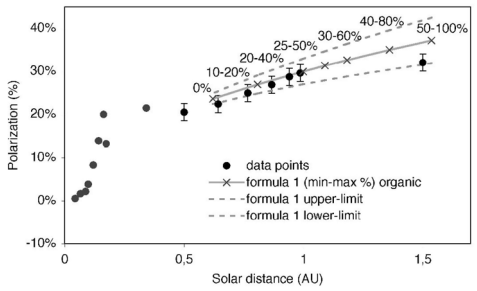

Fig. 4. Dependence of P_{90° on R. Data points (•) are compared to the previous IDC model with a silicate-organic composition expressed as percent of organic (×) varying with the distance to the Sun. Percentage values take the possible presence of core-mantle particles into account. Data points are adapted from Levasseur-Regourd et al. (2001) and references therein. The error bars are shown whenever greater than 0.5%.

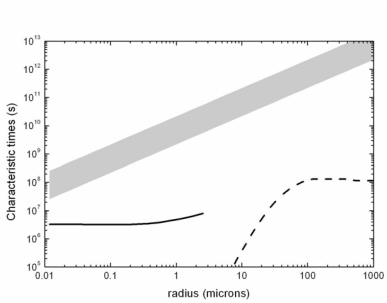

Fig. 5. Comparison between characteristic migration times and characteristic degradation times of spherical particles as a function of their radius. The gray zone corresponds to characteristic migration times of spherical particles submitted to the Poynting-Robertson effect with a density between 1000 kg m^{-3} (upper limit) and 100 kg m^{-3} (lower limit). The dashed and plain lines correspond to the degradation time of POM and poly-HCN particles respectively at 1 AU.

(in the 0.5 to 0 AU range), where a drastic change in polarization is observed.

4.3. Discussion

The light-scattering analysis (Fig. 2) indicates the presence of two types of material (typically non-absorbing silicates and more absorbing carbonaceous material), possibly mixed together in the IDC in the form of silicate-core, organic-mantle particles. It confirms previous studies showing that a significant part of the IDC is generated from cometary dust where these materials have been observed in large quantities (see e.g. Greenberg & Hage 1990). It also agrees with infrared observations showing silicates emission features (see e.g. Reach et al. 1996; Leinert et al. 2002), with the analysis of the IDPs collected in the stratosphere of the Earth and micrometeorites collected in ices (for a review, see Jessberger et al. 2001) and with recent analyses of Stardust samples (see e.g. Zolensky et al. 2006; Sandford et al. 2006). However, it does not rule out the existence of a significant contribution from dust resulting from asteroidal collisions.

Heliocentric dependence analysis (Fig. 4) also shows that a change in the composition of the IDC, with a decrease in the absorbing carbonaceous material percentage when the solar distance decreases, can explain the decrease in P_{90° from 1.5 to 0.5 AU. This interpretation is coherent with previous solar F-corona and zodiacal light data showing a probably wide extended zone of degradation of the carbonaceous material away from the Sun (Mann et al. 1994) reaching up to 1.8 AU (Mukai 1996). It also agrees with recent mid-infrared observations suggesting that the silicates emission feature decreases farther away from the Sun (Reach et al. 2003). It finally supports the decrease in the local albedo value of the particles farther away from the Sun deduced from the observations (Levasseur-Regourd et al. 2001).

This interpretation is also consistent with observations within cometary atmospheres. It has already been shown that solid organic material ejected from cometary nuclei on grains can be degraded when the temperature of the grains rises in the coma. The degradation of polyoxymethylene (formaldehyde polymers: (-CH_2-O-)n, also called POM) has been proposed as the origin of the formaldehyde extended source observed in comet Halley (Cottin et al. 2004). Such a mechanism is also consistent with the variation in the production of H_2CO in comet Hale-Bopp from 0.9 UA to 4 UA (Fray et al. 2006). However, POM is a rather fragile compound, and its degradation would only contribute to a variation in grain composition over a short period of time, inside the coma under thermal effect. From 1.5 to 0.5 AU, the characteristic time of POM disappearance is much lower than the one of migration towards the Sun under the Poynting-Robertson effect. As an example, considering a grain with an effective radius of 100 μm at 1 AU having a black body temperature near 280 K, 99% of POM presumably present in this grain would disappear in about 10^8 s (covering about 10^{-4} UA), whereas its migration time towards the Sun is about 10^{12} s, as can be seen in Fig. 5. Thus, POM cannot explain the dependence of P_{90° on R.

However, other organic compounds, such as HCN polymers (Rettig et al. 1992) have been proposed as part of the solid organic component of cometary grains. Their degradation could be responsible in part for the P_{90° variation. Preliminary results on the thermal degradation of HCN polymers have shown that this compound is much more resistant than POM (Fray et al. 2004) and that it starts to decompose only for temperatures higher than 450 K. Setting this triggering temperature implies that HCN polymer could survive closer to the Sun than POM. Other solid carbonaceous compounds should also be considered, such as amorphous carbon or carbon nitride, for which the onset decomposition temperature is comprised between 600 and 800 K (Zhang et al. 2002). The dependence of P_{90° on R could probably be explained by the degradation of a mixture of refractory compounds, for which degradation is triggered at different temperatures, depending on the grain size and the heliocentric distance.

Although the variation of polarization can be explained well in the 1.5 to 0.5 AU range with the composition change (see Fig. 4), it may be noticed that degradation processes may also change the size distribution but with a limited effect from 1 to 0.1 AU (see e.g. Kimura et al. 1998; Mann et al. 2004). However, other processes are mandatory for explaining the drastic variation of polarization further for R below 0.5 AU. Gail & Sedlmayr (1999) have shown that compounds such as enstatite and forsterite (typically Mg-rich pyroxene and olivine) have their stability limits under equilibrium conditions in the temperature region between 800 K and 1100 K. These temperatures should be reached for distances R to the Sun below 0.3 AU (see e.g. Kimura et al. 2002; Mann et al. 2004). The degradation of silicate minerals in this region could explain the observed variation in the polarization.

The amount of fluffy particles used in our model is about 20% in mass. This may be related to the unfragmented particles originating from comets constituting at least 20% of the IDC in mass. This is only a lower limit value since not all the cometary dust particles present a porous structure (Hörz et al. 2006). Such a result agrees reasonably with previous estimations of the asteroidal to cometary dust ratio deduced from collisional evolution of asteroids (at least 1/3 of IDC is of asteroidal origin, Dermott et al. 1996) and from lunar impact analysis (2/3 is of asteroidal origin, Fechtig et al. 2001).

5. Equilibrium temperature of the particles

The temperature, T, of dust particles in thermal equilibrium at a solar distance, R, typically between 1.5 and 0.5 AU, is computed by making incident and emitted energy equal over the ultraviolet, the visible, and infrared spectrum, from around 0.1 to 1000 μm,

$$\left(\frac{r}{R}\right)^2 \int_0^\infty B(\lambda, T_S) Q_{abs}(a, \lambda) d\lambda = \varsigma \int_0^\infty B(\lambda, T) Q_{abs}(a, \lambda) d\lambda \quad (5)$$

where r is the radius of the Sun, $B(\lambda, T)$ the Planck function, T_S the solar surface temperature, ς the ratio of the emitting surface over $\pi a^2/4$, and $Q_{abs}(a, \lambda)$ the absorption efficiency of a particle with a given optical index $m(\lambda)$ (Kolokolova et al. 2004).

Since the absolute value of T at 1 AU is not accurately known, we mainly discuss the variation of T with R and tentatively reproduce such a variation in the frame of the previous model. Calculations are performed for various shapes: core-mantle spheres, core-mantle prolate spheroids, and the typical fractal aggregates (BCCA and BPCA) of them. The optical indices are taken to be those of astronomical silicates (Draine & Lee 1984), Mg-rich pyroxene (as described in 4.1, Dorschner et al. 1995), refractive organic material (Li & Greenberg 1997), or amorphous carbon (Edoh 1983).

5.1. Results for the temperature of isolated dust particles

Figure 6 presents the variation in the equilibrium temperature with the heliocentric distance in logarithmic scale between 1.5 and 0.5 AU for spheres, spheroids, and 64 spheres BCCA-BPCA aggregates (of 1.5 μm equivalent volume sphere diameter meaning constituting spheres of 0.19 μm radius) made of astronomical silicates, Mg-rich pyroxene, organic, or amorphous carbon material. The curves are systematically compared to the IDC temperature variation (Eq. (2)) retrieved from the observations and the black body temperature. The absolute value of the temperature is approximated better by black body particles, low-absorbing materials (such as Mg-rich pyroxene), and the more compact particles amongst the aggregates. This agrees with previous works (see e.g. Reach et al. 2003; and Kasuga et al. 2006) showing that the particles near 1 AU are rather large and compact with behavior close to a black body. However, the temperature-distance factor, t, between 0.5 and 1.5 AU is approximately equal to −0.33 for organic, −0.35 for amorphous carbon that is significantly closer to the observations (Eq. (2)) than the values of −0.52 for astronomical silicates, and −0.5 for Mg-rich pyroxene. This suggests that absorbing materials constitute a non negligible component of the IDC between 0.5 and 1.5 AU.

The heliocentric power-law dependence of the temperature does not change significantly with the shape of the particle (spheres, spheroids, or BCCA-BPCA aggregates) and is instead

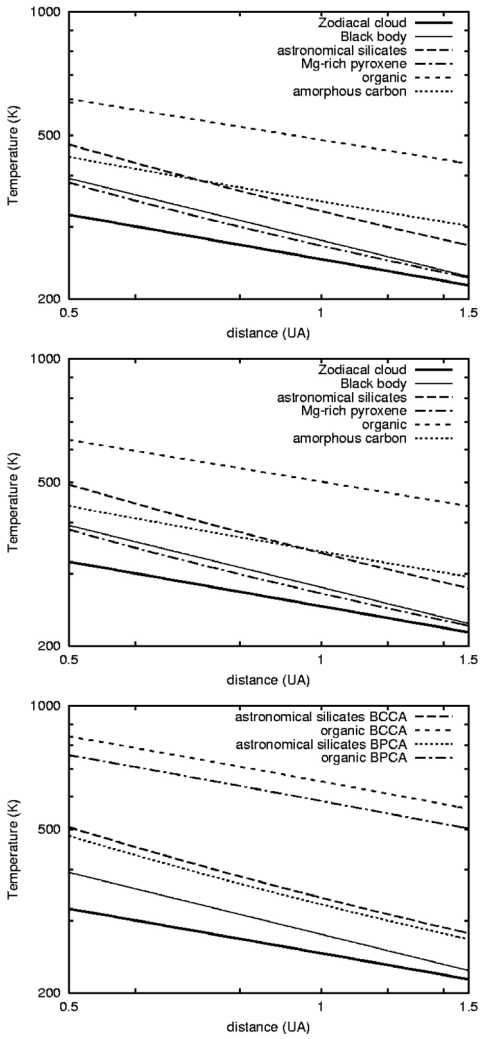

Fig. 6. Logarithmic plot of the dust temperature in the symmetry surface as a function of the solar distance. Temperature is inferred from observations (thick solid line), as compared to black body temperature (thin solid line) and temperature computed for spheres (*top*), spheroids (*middle*), and BCCA-BPCA aggregates (*bottom*) of an equivalent diameter 1.5 μm.

defined by the effective diameter and the material constituting the particle. The variation in t with the size of the particles is not accurately known, but should tend towards a black body law when the equivalent diameter of the particles increases.

Figure 7 shows the comparison between the temperature-distance factors retrieved from the observations (with the estimated error bar represented by a gray zone) and computed for spheres and spheroids as a function of the size of the particles. For an equivalent radius larger than 10 μm, the equilibrium temperature of these particles behaves like the one of a black body. For smaller sizes (<1 μm), the temperature-distance factor, t, of the astronomical silicates and pyroxene particles is around the black body value, whereas for the (more absorbing) organic and carbon material, t is equal to the temperature-distance factor retrieved from the observations within the error bars.

As illustrated in Fig. 6, the temperatures obtained for more absorbant materials (organic and amorphous carbon) are higher than those corresponding to less absorbant materials (astronomical silicates and Mg-rich pyroxene) for the same equivalent radius. This corresponds to the fact that organic or carbon particles

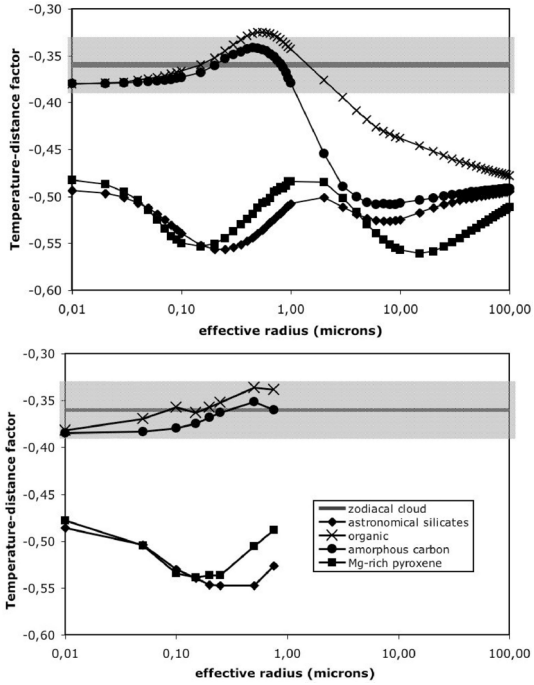

Fig. 7. Comparison between temperature-distance factors in the symmetry surface and between 0.5 and 1.5 AU, as inferred from observations (thick solid line surrounded by gray zone) and as calculated for spheres (top) and spheroids (bottom) as a function of their equivalent radius. Calculations are presented for astronomical silicates (♦), Mg-rich pyroxene (■), and absorbing material like organic (×), and amorphous carbon (●) material.

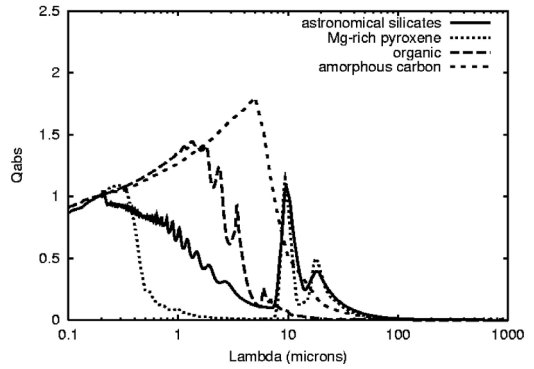

Fig. 8. Comparison of absorption efficiency, $Q_{\rm abs}$, for spheres made of different materials (astronomical silicates, Mg-rich pyroxene, organic, amorphous carbon) as a function of the wavelength for an equivalent radius of 0.75 μm.

absorb more than the silicates in the visible and the near infrared part of the spectrum, whereas they emit less in the infrared, as can be seen in Fig. 8 that shows the absorption efficiency of spherical particles of radius 0.75 μm.

Higher values of the temperature are obtained for fluffier particles: BCCA compared to BPCA aggregates, and aggregates compared to equal volume spheroids. This indicates the importance of the size and porosity of the particles for their equilibrium temperature and results from the fact that the more porous an aggregate is, the lower the contribution of the interaction between constituent particles, and the more prominent the properties of its individual, constituent particles (in agreement with Xing & Hanner 1997; and Kolokolova et al. 2007).

5.2. Equilibrium temperature of a cloud of spherical particles

5.2.1. Principles of the emissivity calculation of the particles

The emissivity, ε_λ, of a cloud of particles with different compositions at a given wavelength and distance to the Sun is obtained by summing the Planck function contribution of each particle (with a temperature, T, and an absorption efficiency, $Q_{\rm abs}$, depending on its size). These considerations are summed up in the following equation from Reach et al. (2003):

$$\varepsilon_\lambda = \sum_i \int \Gamma(a)^{(i)} B_\lambda \left(T^{(i)}(a)\right) \pi a^2 Q^{(i)}_{\rm abs}(a,\lambda) {\rm d}a, \quad (6)$$

where the sum over i corresponds to the sum over the different materials constituting the cloud, a is the equivalent diameter of the particles, and $B_\lambda \left(T^{(i)}(a)\right)$ is the value of the Planck function at a given temperature, $T^{(i)}(a)$, and a given wavelength, λ; and $\Gamma(a)$ is the same size distribution of particles than the one deduced from the polarization calculations in Part 4. To be able to compare the emissivity with Planck curves, the above integral is normalized:

$$\langle \varepsilon_\lambda \rangle = \sum_i \frac{\int \Gamma(a)^{(i)} B_\lambda \left(T^{(i)}(a)\right) \pi a^2 Q^{(i)}_{\rm abs}(a,\lambda) {\rm d}a}{\int \Gamma(a)^{(i)} \pi a^2 Q^{(i)}_{\rm abs}(a,\lambda) {\rm d}a}. \quad (7)$$

And $\langle \varepsilon_\lambda \rangle$ depends on the distance to the Sun, since the temperature of the particles varies with this parameter.

5.2.2. Heliocentric variation in the brightness temperature

The variation in the absorption efficiency with the wavelength implies that particles with a radius smaller than 0.1 μm absorb and emit very little, and thus do not contribute much to the emissivity function (see e.g. Reach 1988). Particles with a size less than 1 μm, generally have a much higher equilibrium temperature than the black body one as shown in Fig. 9, while particles with a radius larger than 10 μm have an emissivity close to the black body one.

This behavior, already perceptible in the behavior of the temperature-distance factor as a function of the particles radius (Fig. 7), is confirmed in Fig. 9, which shows the variation in the equilibrium temperature of the spheres as a function of their radius at a given solar distance (0.5, 1, and 1.5 AU). Particles with radius smaller than 1 μm have higher temperatures and particles with a radius larger than 10 μm have temperatures similar to a black body.

The approximation of the emissivity curve $\langle \varepsilon_\lambda \rangle$ by a Planck curve over the whole visible and infrared spectrum (from $\approx$0.1 μm to $\approx$1000 μm) gives the equivalent of the brightness temperature of the cloud of particles, which corresponds to the temperature of the black body that best fits the particles' cloud spectrum. This temperature calculated at different distances to the Sun gives the temperature-distance factor of the particle cloud. Temperatures and temperature-distance factors depending on the distance to the Sun are presented in the Tables 1 and 2.

The variation in the brightness temperature with the distance to the Sun depends strongly on the material. The calculations presented in Table 2 confirm that a cloud of silicate particles behave like a black body, whereas the temperature-distance factor has lower values for a cloud of particles constituted of more absorbing materials (organic and amorphous carbon).

The results of the brightness temperature obtained for a mixture of organic and astronomical silicates between 0.5 AU and

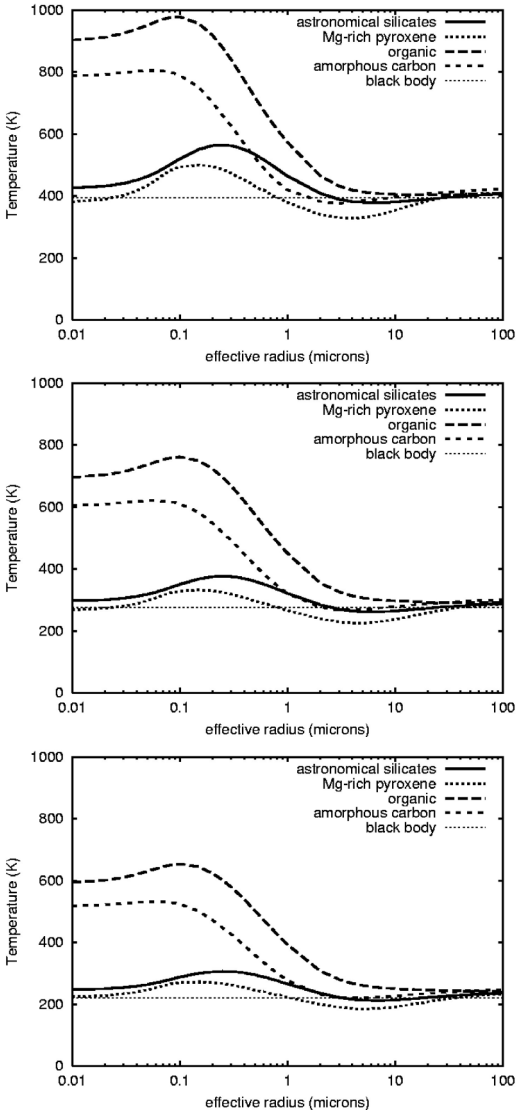

Fig. 9. Equilibrium temperature of spheres as a function of their radius and their constituent materials. The curves are computed for different solar distances: 0.5 AU (*top*), 1 AU (*middle*), 1.5 AU (*bottom*).

1.5 AU show that a mixture including approximately 50% of organic and 50% of astronomical silicates in mass as deduced from the previous light-scattering study can explain a significantly different behavior from a black body with a temperature-distance factor $t = -0.45$. The same temperature-distance factor would also be found if we considered only silicates material at 0.5 AU since the brightness temperature of the mixture of silicates and organic is close to the one of silicates at this distance (see Table 1). This result confirms the previous estimations of the composition of the IDC from the light-scattering observations.

5.3. Discussion

The temperature-distance factor retrieved from the light-scattering observations differs from the black body law. It is possible that the emitting particles may be small and irregular scatterers, for which the black body approximation cannot be used. Also, t does not change significantly with the shape of the particle (spheres, spheroids, or aggregates) and is mostly defined by the effective diameter and the material constituting the particle, in agreement with previous temperature calculations for amorphous carbon (Xing & Hanner 1997). The equilibrium temperature obtained for silicate particles decreases faster with R than for absorbing particles, as can be expected from the presence of silicate emission features in the infrared (Mann et al. 1994). This can also explain the lower temperature obtained for silicates as compared to more absorbing material in Fig. 6.

In agreement with Xing & Hanner (1997), the temperature obtained for an aggregate of grains is lower than one of its constituent grains but is higher than the temperature of the equivalent volume sphere. The temperature and polarization thus behave in opposite ways because a fluffy aggregate of small grains presents values of t close to the one of its equivalent volume sphere, whereas it scatters light in a similar way to one of its constituent grains as shown from numerical simulations (West 1991) and experimental simulations (Wurm et al. 2004).

The works of Reach et al. (1988, 2003) use different sphere size distributions (power law, interplanetary dust size distribution, Hanner cometary dust size distribution, etc.) and material similar to the ones we considered here (astronomical silicates, andesite, obsidian, amorphous and crystalline olivine, amorphous and crystalline pyroxene, carbon, etc.). Their study shows a best fit with the observations for a mixture of 10% carbon and 90% silicates and the interplanetary dust particles size distribution, which gives more weight to the particles in the 10 to 100 μm diameter. The conclusions presented in this work agree fairly with their model, but it has been developed specifically to try to interpret the peculiar variation in the temperature with the heliocentric distance.

6. Conclusions

The physical properties of the interplanetary dust cloud in the near ecliptic symmetry surface are tentatively derived from scattered and emitted light observations. Results for the composition of the dust cloud, the size distribution, and the shape of the particles are summarized below.

1. Both silicates and (more absorbing) organic materials are necessary to explain the local polarization and temperature values retrieved from observations, as well as their variation with the solar distance.
2. A good fit of the polarization phase curve available near 1.5 AU is obtained for a realistic particle size distribution (with a power law a^{-3} for particles with an equivalent diameter, a, between 0.22 μm and 20 μm and $a^{-4.4}$ for larger particles) and for a mixture of silicates and more absorbant organic materials (between 20% and 60% in mass).
3. The upper cutoff of the size distribution is not well-constrained with the above-mentioned size distribution, allowing the presence of rather large, compact particles.
4. The decrease in P_{90° with the solar distance between 1.5 and 0.5 AU is interpreted as a progressive disappearance of the solid carbonaceous compounds (such as HCN polymers or amorphous carbon) towards the Sun, probably linked with the presence of an extended zone of thermal degradation.
5. The drastic change in P_{90° closer to the Sun between 0.5 and 0 AU could be explained by other physical processes, such as the degradation of silicate materials or a change in the size distribution possibly favoring smaller particles towards the Sun.
6. Unfragmented aggregates of cometary origin that contribute to the interplanetary dust cloud are of at least 20% in mass around 1.5 AU.

Table 1. Brightness temperature as a function of the distance to the Sun, R, for a cloud of spherical particles with the size distribution obtained in Part 4.

R	Observations	Astronomical silicates	Mg-rich pyroxene	Organic	Amorphous carbon	50% silicates– –50% organic	Black body
0.5 AU	321 ± 20 K	414 K	371 K	524 K	471 K	408 K	394 K
1 AU	250 ± 10 K	295 K	255 K	388 K	351 K	298 K	279 K
1.5 AU	216 ± 11 K	243 K	210 K	327 K	299 K	249 K	228 K

Table 2. Brightness temperature-distance factor, t, for a cloud of spherical particles with the size distribution obtained in Part 4, where t is calculated over three domains (between 0.5 and 1.5 AU).

Domain (AU)	Observations	Astronomical silicates	Mg-rich pyroxene	Organic	Amorphous carbon	50% silicates– –50% organic	Black body
0.5–1	−0.36 ± 0.03	−0.49	−0.54	−0.43	−0.43	−0.45	−0.5
1–1.5	−0.36 ± 0.03	−0.48	−0.49	−0.42	−0.39	−0.44	−0.5
0.5–1.5	−0.36 ± 0.03	−0.48	−0.52	−0.43	−0.41	−0.45	−0.5

7. The size distribution retrieved from the polarization fit leads to a temperature variation in $R^{-0.45}$ different from the black body behavior and closer to the observations.
8. The variation in the temperature with the solar distance for absorbing materials is closer to the observations than the one of non absorbing materials. This behavior is mainly due to particles with a diameter smaller than 2 μm.

Acknowledgements. This research has been partially funded by the French space agency (CNES). The authors acknowledge fruitful discussions with J.-B. Renard and helpful comments from an anonymous referee.

References

Bockelée-Morvan, D., Gautier, D., Hersant, F., Huré, J.-M., & Robert, F. 2002, A&A, 384, 1107
Bradley, J. P., Humecki, H. J., & Germani, M. S. 1992, ApJ, 394, 643
Cottin, H., Bénilan, Y., Gazeau, M.-C., & Raulin, F. 2004, Icarus, 167, 397
Dermott, S. F., Grogan, K., Gustafson, B. A. S., et al. 1996, in Physics, Chemistry and Dynamics of Interplanetary Dust, ed. B. A. S. Gustafson, & M. S. Hanner, ASP Conf. Ser., 104, 143
Dermott, S. F., Grogan, K., Durda, D.D., et al. 2001, in Interplanetary dust, ed. E. Grün, B. A. S. Gustafson, S. Dermott, & H. Fechtig, 569
Dorschner, J., Begemann, B., Henning, Th., Jäger, C., & Mutschke, H. 1995, A&A 300, 503
Draine, B. T., & Lee, H. M. 1984, ApJ, 285, 89
Draine, B. T., & Flatau, P. J. 2000, `http://arxiv.org/abs/astro-ph/0008151v4`
Dumont, R., & Levasseur-Regourd, A. C. 1988, A&A, 191, 154
Edoh, O. 1983, Optical Properties of Carbon from the Far Infrared to the Far Ultraviolet, Ph.D. Thesis (University of Arizona Press)
Engrand, C., & Maurette, M. 1998, M&PS, 33, 565
Fechtig, H., Leinert, Ch., & Berg, O. E. 2001, in Interplanetary Dust, ed. E. Grün, B. A. S. Gustafson, S. Dermott, & H. Fechtig (Springer-Verlag), 1
Flynn, G. J., Keller, L. P., Jacobsen, C., & Wirick, S. 2004, Adv. Space Res., 33, 57
Fray, N., Bénilan, Y., Cottin, H., et al. 2004, M&PS, 39, 581
Fray, N., Bénilan, Y., Biver, N., et al. 2006, Icarus, 184, 239
Gail, H.-P., & Sedlmayr, E. 1999, A&A, 347, 594
Greenberg, J. M., & Hage, J. I. 1990, ApJ, 361, 260
Grün, E., Zook, H.A., Baguhl, M., et al. 1993, Nature, 362, 428
Grün, E., Baguhl, M., Svedhem, H., & Zook, H. A. 2001, in Interplanetary Dust, ed. E. Grün, B. A. S. Gustafson, S. Dermott, & H. Fechtig (Springer-Verlag), 295
Hanner, M. S., & Bradley, J. P. 2004, in Comets II, ed. M. C. Festou, H. U. Keller, & H. A. Weaver (University of Arizona Press), 555
Hanner, M. S., Veeder, G. J., & Tokunaga, A. T. 1992, AJ, 104, 386
Hayward, T. L., Hanner, M. S., & Sekanina, Z. 2000, ApJ, 538, 428
Hellyer, B. 1970, MNRAS, 148, 383
Hörz, F., Bastien, R., Borg, J., et al. 2006, Science, 314, 1716
Jäger, C., Molster, F. J., Dorschner, J., et al. 1998, A&A, 339, 904
Jenniskens, P. 1993, A&A, 274, 653
Jessberger, E. K., Stephan, T., Rost, D., et al. 2001, in Interplanetary Dust, ed. E. Grün, B. A. S. Gustafson, S. Dermott, & H. Fechtig (Springer-Verlag), 253
Jorda, L., Lamy, P., Faury, G., et al. 2007, Icarus, 187, 208
Kasuga, T., Yamamoto, T., Kimura, H., & Watanabe, J. 2006, A&A, 453, L17
Keller, L. P., Thomas, K. L., & McKay, D. S. 1994, in Analysis of Interplanetary Dust, ed. M. E. Zolensky, T. L. Wilson, F. J. M. Rietmeijer, & G. J. Flynn, AIP Conf. Proc., 310, 159
Kimura, H. 2001, JQSRT, 70, 581
Kimura, I., Mann, I., & Mukai, T. 1998, Planet. Space Sci., 46, 911
Kimura, I., Mann, I., Biesecker, D.A., & Jessberger, E.K. 2002, Icarus, 159, 529
Kolokolova, L., Hanner, M. S., Levasseur-Regourd, A. C., & Gustafson, B. A. S. 2004, in Comets II, ed. M. C. Festou, H. U. Keller, & H. A. Weaver (University of Arizona Press), 577
Kolokolova, L., Kimura, H., Kiselev, N., & Rosenbush, V. 2007, A&A 463, 1189
Lasue, J., & Levasseur-Regourd, A. C. 2006, JQSRT, 100, 220
Leinert, Ch., Bowyer, S., Haikala, L. K., et al. 1998, A&AS, 127, 1
Leinert, Ch., Ábrahám, P., Acosta-Pulido, J., Lemke, D., & Siebenmorgen, R. 2002, A&A, 393, 1073
Levasseur-Regourd A.C. 2003, Adv. Space Res., 31, 2599
Levasseur-Regourd, A. C., & Hadamcik, E. 2003, JQSRT, 79, 903
Levasseur-Regourd, A. C., Cabane, M., & Haudebourg, V. 1999, JQSRT, 63, 631
Levasseur-Regourd, A. C., Mann, I., Dumont, R., & Hanner, M. S. 2001, in Interplanetary Dust, ed. E. Grün, B. A. S. Gustafson, S. Dermott, & H. Fechtig (Springer-Verlag), 57
Levasseur-Regourd, A. C., Mukai, T., Lasue, J., & Okada, Y. 2007, Planet. Space Sci., 55, 1010
Li, A., & Greenberg, J. M. 1997, A&A, 323, 566
Lucey, P. G. 1998, JGR, 103, E1, 1703
Lumme, K. 2000, in Light scattering by non spherical particles, ed. M. I. Mishchenko, J. W. Hovenier, & L. D. Travis (San Diego: Academic Press), 555
Macke, A., & Mishchenko, M. I. 1996, App. Opt., 35, 4291
Mann, I. 1992, A&A, 261, 329
Mann, I., Okamoto, H., Mukai, T., Kimura, H., & Kitada, Y. 1994, A&A, 291, 1011
Mann, I., Kimura, I., Biesecker, D.A., et al. 2004, Space Sci. Rev., 110, 269
Meakin, P. 1983, Phys. Rev. Lett., 51, 1119
Mishchenko, M. I., & Travis, L. D. 1998, JQSRT, 60, 309
Mukai, T. 1996 in Physics, Chemistry and Dynamics of Interplanetary Dust, ed. B. A. S. Gustafson, & M. S. Hanner, ASP Conf. Ser., 104, 453
Mukai, T., Blum, J., Nakamura, A. M., Johnson, R. E., & Havnes, O. 2001, in Interplanetary Dust, ed. E. Grün, B. A. S. Gustafson, S. Dermott, & H. Fechtig (Springer-Verlag), 445
Papoular, R., Breton, J., Gensterblum, G., et al. 1993, A&A, 270, L5
Reach, W. T. 1988, ApJ, 335, 468
Reach, W. T. 1991, ApJ, 369, 529
Reach, W. T., Abergel, A., Boulanger, F., et al. 1996, A&A, 315, L381
Reach, W. T., Morris, P., Boulanger, F., & Okumura, K. 2003, Icarus, 164, 384
Renard, J. B., Levasseur-Regourd, A. C., & Dumont, R. 1995, A&A, 304, 602
Rettig, T. W., Tegler, S. C., Pasto, D.J., & Mumma, M. J. 1992, ApJ, 398, 293
Sandford, S. A., Aléon, J., Alexander, C. M. O'D., et al. 2006, Science, 314, 1720
West, R. A. 1991, App. Opt., 30, 5316
Whipple, F.L. 1951, ApJ, 113, 464
Wooden, D. H., Harker, D. E., Woodward, C. E., et al. 1999, ApJ, 517, 1034
Wurm, G., Relke, H., Dorschner, J., & Krauss, O. 2004, JQSRT, 89, 371
Xing, Z., & Hanner, M. 1997, A&A, 324, 805
Zhang, L. H., Gong, H., & Wang, J. P. 2002, J. Phys. Cond. Matter, 14, 1697
Zolensky, M. E., Zega, T. J., Yano, H., et al. 2006, Science, 314, 1735